

The Optical Light Curves of Cygnus X-2 (V1341 Cyg) and the Mass of its Neutron Star

Jerome A. Orosz¹ & Erik Kuulkers^{2*}

¹*Department of Astronomy & Astrophysics, The Pennsylvania State University, 525 Davey Laboratory, University Park, PA 16802, USA*

²*Astrophysics, University of Oxford, Nuclear and Astrophysics Laboratory, Keble Road, Oxford OX1 3RH, UK*

25 March 2018

ABSTRACT

We present U , B and V light curves (taken from the literature) of the low mass X-ray binary Cygnus X-2. We show that the most significant photometric periods seen in the B and V light curves are consistent with half of the orbital period found from spectroscopy ($P = 9.8444$ days). The “lower envelope” of the light curves folded on the orbital period are ellipsoidal (i.e. they have two maxima and two minima per orbital cycle). We fit an ellipsoidal model to the lower envelopes of the B and V light curves to derive inclination constraints. This model includes light from an accretion disc and accounts for eclipses and X-ray heating. Using the extreme assumption that there is no disc light, we derive a lower limit on the inclination of $i \geq 49^\circ$. If we assume the accretion disc is steady-state where its radial temperature profile goes as $T(r) \propto r^{-3/4}$, we find an inclination of $i = 62.5^\circ \pm 4^\circ$. However, the predicted ratio of the disc flux to the total flux in B (the “disc fraction”) is larger than what is observed (≈ 0.55 compared to ≤ 0.3). If we use a flatter radial temperature profile of the disc expected for strongly irradiated discs ($T(r) \propto r^{-3/7}$), then we find an inclination of $i = 54.6^\circ$ and a disc fraction in B of ≈ 0.30 . However, in this case the value of χ^2 is much larger (48.4 with 36 degrees of freedom compared to 40.9 for the steady-state case). Adopting $i = 62.5 \pm 4^\circ$ and using a previous determination of the mass ratio ($q = M_c/M_x = 0.34 \pm 0.04$) and the optical mass function ($f(M) = 0.69 \pm 0.03 M_\odot$), we find that the mass of the neutron star is $M_x = 1.78 \pm 0.23 M_\odot$ and the mass of the secondary star is $M_c = 0.60 \pm 0.13 M_\odot$. We derive a distance of $d = 7.2 \pm 1.1$ kpc, which is significantly smaller than a recent distance measurement of $d = 11.6 \pm 0.3$ kpc derived from an observation of a type I radius-expansion X-ray burst, but consistent with earlier distance estimates.

Key words: binaries: close — stars: individual (Cygnus X-2, V1341 Cygni) — X-rays: stars

1 INTRODUCTION

Reliable measurements of neutron star masses are important for placing constraints on the equation of state of dense nuclear matter. Currently, the most precise mass measurements for neutron stars come from studies of binary radio pulsars (Stairs et al. 1998; Thorsett & Chakrabarty 1998). The masses of the neutron stars in the binary radio pulsars likely reflect the mass at their formation since these particular neutron stars presumably have not accreted any mass since their formation. On the other hand, neutron stars in X-ray binaries have been accreting at large rates for extended periods of time. Hence the mass estimates for neu-

tron stars in X-ray binaries should give us information on the *range* of allowed masses (van Kerkwijk, van Paradijs, & Zuiderwijk 1995a; van Paradijs 1998). Unfortunately, X-ray binaries are not as “clean” as binary radio pulsars and mass determinations derived from dynamical studies are subject to larger uncertainties (e.g. van Kerkwijk et al. 1995b; Stickland, Lloyd, & Radziun-Woodham 1997). In the case of the high-mass X-ray binaries, the observed radial velocity curves often show pronounced deviations from the expected Keplerian shapes, presumably due to tidal effects and non-radial oscillations in the high-mass secondary star. Since most of the mass of the binary resides in the high-mass O/B secondary star, the derived neutron star masses are quite sensitive to errors in the velocity curves of the visible stars. In the case of many low-mass X-ray binaries, it is often not possible to directly observe the secondary star optically since

* Present address: Space Research Organization Netherlands, Sorbonnelaan 2, 3584 CA Utrecht, The Netherlands

the accretion disc dominates the observed flux. Hence, reliable dynamical mass estimates are not available for many of these systems.

Cygnus X-2, which is one of the brightest low-mass X-ray binaries known, is one of the rare cases among the persistent low-mass X-ray binaries where the secondary star is easily observed. Cyg X-2 is known to contain a neutron star because Type I X-ray bursts have been observed (Kahn & Grindlay 1984; Kuulkers, van der Klis, & van Paradijs 1995; Wijnands et al. 1997; Smale 1998). The neutron star is believed to be accreting mass from its companion at a near Eddington rate (see Smale 1998). V1341 Cygni, its optical counterpart (Giacconi et al. 1967), is relatively bright, so reasonably precise spectroscopic and photometric observations can be obtained. The orbital period of $P = 9.844$ days was determined by Cowley et al. (1979) and by Crampton & Cowley (1980) from the observed radial velocity variations of the companion star. Cowley et al. (1979) also reported a spectral type for the companion star in the range of A5 to F2 (they attributed the change in the observed spectral type to X-ray heating of the secondary). Casares, Charles, & Kuulkers (1998, hereafter CCK98) have recently refined the measurements of the orbital parameters. They determined a period of $P = 9.8444 \pm 0.0003$ days, an optical mass function of

$$f(M) \equiv \frac{PK_c^3}{2\pi G} = \frac{M_x \sin^3 i}{(1+q)^2} = 0.69 \pm 0.03 M_\odot, \quad (1)$$

where M_x is the mass of the neutron star, M_c is the mass of the companion star, K_c is the semi-amplitude of the companion's radial velocity curve, and where $q = M_c/M_x = 0.34 \pm 0.04$. CCK98 also determined a spectral type for the companion star of A9III and reported no variation of the spectral type with orbital phase, in contradiction to Cowley et al. (1979).

One needs a measurement of the orbital inclination in order to derive mass measurements from the orbital elements of CCK98. Models of the optical/IR light curves are the most “direct” method to determine the inclination (e.g. Avni & Bahcall 1975; Avni 1978). We have gathered U , B , and V photometric data of Cyg X-2 from the literature with the goal of obtaining the mean light curve and deriving the inclination. We demonstrate that the derived mean orbital light curves show the familiar signature of ellipsoidal variations. The light curves are then modeled to place limits on the inclination. We also show that the photometric period is consistent with the spectroscopic orbital period. We describe below the analysis of the tabulated photometric data, period determination, and the ellipsoidal modelling. We conclude with a discussion of the mass of the neutron star and the distance to the source.

2 CYG X-2 LIGHT CURVES

2.1 Observations

We used all the photoelectric and photographic data as tabulated in the literature for our analysis. These are photoelectric (U , B , and V) data obtained between 1967 and 1984 (Kristian et al. 1967; Peimbert et al. 1968; Mumford 1970; Chevalier, Bonazzola & Ilovaisky 1976; Lyutyi & Sunyaev 1976; Ilovaisky et al. 1978; Kilyachkov 1978; Beskin

et al. 1979; Goranskii & Lyutyi 1988), and photographic (B and V) data obtained in 1974 and 1975 (Basko et al. 1976). The uncertainties of the photoelectric data are typically between 0.02–0.03 magnitudes in the V and B band, and 0.05–0.08 magnitudes in the U band, while the photographic data have typical uncertainties between 0.08–0.15 magnitudes (see Goranskii & Lyutyi 1988). Close B and V photographic magnitudes in time with B and V photoelectric magnitudes show their measurements to be consistent with each other; we therefore combined them. The mean U , B and V band magnitudes (with the rms given in brackets) of Cyg X-2 from our sample are 14.95 (0.31), 15.16 (0.20), and 14.70 (0.21), respectively.

2.2 Period analysis

Although several periodicities had been reported between ~ 0.25 and ~ 14 days before 1979, none of them were consistent with the orbital period as determined from the spectroscopic observations by Cowley et al. (1979) and Crampton & Cowley (1980) (see also CCK98). After 1979 it was shown that folding the photoelectric and photographic data on the spectroscopic period gave an ellipsoidal (i.e. double-peaked) shaped light curve (Cowley et al. 1979; Goranskii & Lyutyi 1988). Still up to today, no period analysis of the Cyg X-2 light curves has given independent proof of the orbital variations.

We therefore subjected all the combined U (469 points), B (966 points), and V (572 points) band data separately to a period analysis using various techniques (e.g., Lomb-Scargle and phase dispersion minimization). We searched the data for periodicities between 0.1 and 1000 days. Plots of the Lomb-Scargle periodograms can be found in the upper panels of Figure 1. In the figure we also give the 3σ confidence level, above which we regard signals as significant. These confidence levels were determined from a cumulative probability distribution appropriate for our three data sets (see e.g. Homer et al. 1996). The most significant peak found in both the B and V band data were at a period of ~ 4.92 days, whereas no significant peak near this period was found in the U band data. In the lower panels of Figure 1 we give the power spectra of the corresponding window functions in the three passbands. Clearly, the most significant peak in the U band is due to the observing window.

We estimated the error on the periods found by employing a Monte-Carlo technique; we generated $\sim 10,000$ data sets with the same variance, amplitude and period as the observed data. We then subjected the faked data sets to the Lomb-Scargle algorithm; the distribution of the most significant peaks then leads to 1σ error estimates. We also fitted a sine wave to the data near the found periods, where the errors in the magnitude measurements were scaled so that the fit had a reduced χ^2 of ~ 1 ; the 1σ uncertainty in the period was determined using $\Delta\chi^2 = 1$. This resulted in similar error estimates. We derived $P_V = 4.9200 \pm 0.0008$ days, and $P_B = 4.9213 \pm 0.0009$ days. Clearly the period found in the B and V band data is half the (spectroscopic) orbital period. Our analysis therefore gives the first independent proof of (half) the orbital period.

No clear peak can be found near the ~ 78 day X-ray period (Wijnands, Kuulkers & Smale 1996; see also Kong, Charles & Kuulkers 1998). However, other significant peaks

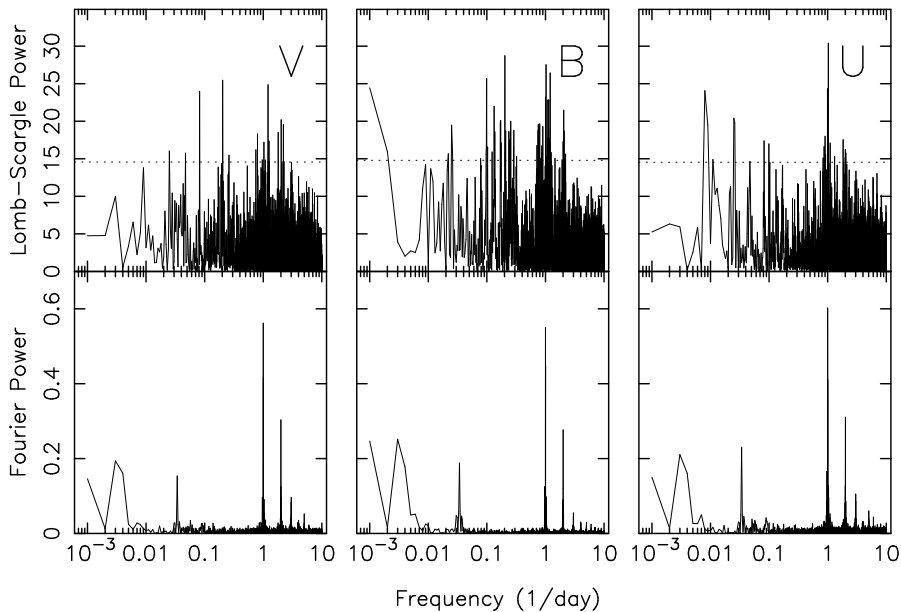


Figure 1. Top panels: The Lomb-Scargle periodograms for the entire V data set (left); the entire B data set (middle), and the entire U data set (right). Bottom panels: The Fourier transforms of the window functions of the three data sets.

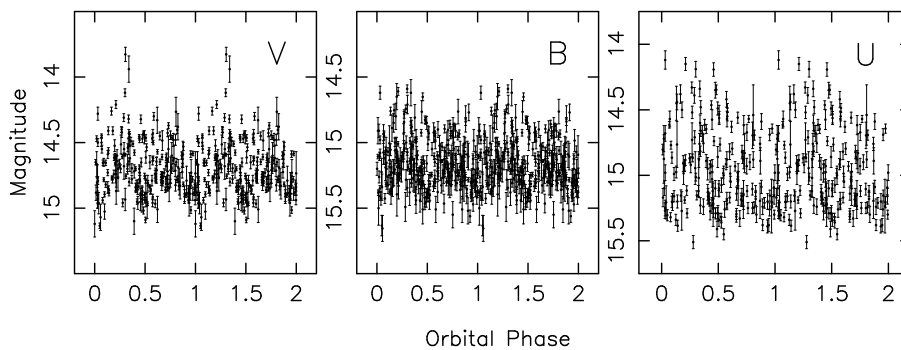


Figure 2. The folded light curves for V (left); B (middle), and U (right). Each point has been plotted twice.

are found at e.g. ~ 12.1 and ~ 35.3 days in V , ~ 10.1 and ~ 39 days in B , ~ 10.1 , ~ 12.1 , ~ 35.3 and ~ 125 days in U , and at aliases between the different periods (e.g. the peak at ~ 0.82 days in V is the alias of half the orbital period and the ~ 35.3 days period). We note that the ~ 35 day period is close to the second significant peak in X-rays reported by Wijnands et al. (1996).

2.3 Mean light curve

Since only the B and V band data shows significant orbital variations, we will concentrate only on mean light curves from these two bands. As noted by Goranskii & Lyutyi (1988), Cyg X-2 shows a strong concentration of data points towards the lowest magnitudes, which they called the “quiet state” (see Figure 1 of Goranskii & Lyutyi 1988 and Figure 2). On top of that Cyg X-2 displays increases in brightness on time-scales ranging from ≈ 5 days to ≈ 10 days, flares lasting less than a day, and drops in brightness for a few days (Goranskii & Lyutyi 1988).

As can be seen in Figure 2, the lower envelope of the data points shows most clearly the ellipsoidal modulations. Rather than constructing mean light curves from data se-

lected from prolonged quiet states in the B band (Goranskii & Lyutyi 1988), we used a more unbiased method.

We computed nightly averages of the observed times and magnitudes, in order to avoid larger weights to nights with many measurements. The nightly averages were phase folded on the ephemeris given by Crampton & Cowley (1980), where we used the definition for phase zero as inferior conjunction of the companion star, which is the time at which the companion star is closest to us. The nightly averages were binned into 20 phase bins, and we determined the lower envelope of the curve by taking the first 6 lowest magnitudes per bin. We then fitted a sine wave to the lower envelope, and subtracted it from the nightly averages. Finally, we discarded those data points which were greater than ≈ 13 times and ≈ 9 times the rms in the mean of the whole sine subtracted data sample, for the B and V band, respectively (there was very little change in the mean light curve when slightly different thresholds were used). The resulting mean B and V band folded light curves of the accepted nightly averages, which corresponds to the so-called “quiescent state”, are shown in Figure 3. We present the folded B and V light curves in tabular form in Tables 1 and 2, respectively.

Table 1. The adopted folded *B* light curve

Phase	<i>B</i> magnitude	magnitude error
0.040	15.350	0.035
0.097	15.289	0.031
0.147	15.275	0.024
0.205	15.180	0.022
0.245	15.155	0.022
0.300	15.206	0.049
0.349	15.196	0.018
0.404	15.279	0.022
0.447	15.309	0.024
0.503	15.400	0.017
0.548	15.300	0.021
0.600	15.248	0.032
0.657	15.208	0.021
0.704	15.222	0.018
0.746	15.187	0.025
0.793	15.219	0.026
0.845	15.234	0.023
0.889	15.320	0.027
0.950	15.333	0.021
0.997	15.314	0.025

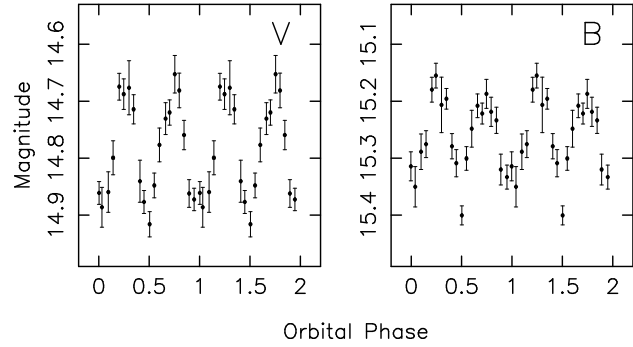
Table 2. The adopted folded *V* light curve

Phase	<i>V</i> magnitude	magnitude error
0.003	14.861	0.020
0.032	14.886	0.035
0.094	14.859	0.036
0.142	14.799	0.030
0.203	14.674	0.024
0.248	14.688	0.027
0.301	14.676	0.047
0.346	14.714	0.026
0.409	14.840	0.037
0.449	14.877	0.020
0.505	14.916	0.022
0.550	14.848	0.022
0.602	14.777	0.030
0.663	14.731	0.028
0.703	14.720	0.022
0.755	14.653	0.033
0.798	14.681	0.030
0.846	14.759	0.026
0.896	14.862	0.024
0.946	14.872	0.020

3 ELLIPSOIDAL VARIATIONS

3.1 Introduction and outline of model

The folded light curves shown in Figure 3 have the well-known signature of ellipsoidal modulations with maxima at phases 0.25 and 0.75 (the quadrature phases) and minima at phases 0.0 and 0.50 (the conjunction phases). The origin of ellipsoidal variations is easy to understand. The secondary star fills its critical Roche lobe (there is ongoing mass transfer) and hence is greatly distorted. As it moves around in its orbit its projected area on the sky (and hence the total observed flux) changes. If the secondary star fills its Roche

**Figure 3.** The final folded and binned “quiescent” light curves for *V* (left); and *B* (right). Each point has been plotted twice.

lobe and is in synchronous rotation, then the amplitude of its ellipsoidal light curve is only a function of the orbital inclination ($i = 90^\circ$ for a system seen edge-on) and the binary mass ratio. Thus models of the ellipsoidal variations offer a way to measure the inclination and mass ratio. However, the *observed* light curve may not be totally due to ellipsoidal modulations from the secondary star. For example, the addition of a substantial amount of extra light from the accretion disc will reduce the overall observed light curve amplitude. X-ray heating of the secondary star can sometimes radically alter the shape of the observed light curve (Avni & Bahcall 1975; Avni 1978). One must therefore account for extra sources of light when modelling X-ray binary (optical) light curves. The folded light curves shown in Figure 3 show the secondary star in Cyg X-2 with the least contamination from the accretion disc (and possibly the least effects of the irradiation). It has already been shown that using the lower envelope of the folded light curve for inclination estimates is a good approximation, when compared to ellipsoidal variations with no disc or irradiation contamination (e.g. Pavlenko et al. 1996). We will discuss below models of the folded light curves shown in Figure 3 and the inclination (and hence mass) constraints we derive from them.

We modeled the light curves using the modified version of the Avni (1978) code described in Orosz & Bailyn (1997). This code uses full Roche geometry to describe the shape of the secondary star. In addition, the code accounts for light from a circular accretion disc and for extra light from the secondary star due to X-ray heating. The parameters for the model are the parameters which determine the geometry of the system: the mass ratio $Q = M_x/M_c^\dagger$, the orbital inclination i , the Roche lobe filling factor f , and the rotational velocity of the secondary star; the parameters which determine the light from the secondary star: its polar temperature T_{pole} , the linearized limb darkening coefficients $u(\lambda)$, and the gravity darkening exponent β ; the parameters which determine the contribution of light from the accretion disc: the disc radius r_d , flaring angle of the rim β_{rim} , the temperature at the outer edge T_d , and the exponent on the power-law radial distribution of temperature ξ , where $T(r) = T_d(r/r_d)^\xi$; and parameters related to the X-ray heating: the X-ray lu-

[†] Following Avni, we use in this section the upper case Q to denote the mass ratio defined by the mass of the compact star divided by the mass of the secondary star. CCK98 and others use the lower case q to denote the inverse.

minosity of the compact object L_x , the orbital separation (determined from the optical mass function, the mass ratio, and the inclination), and the X-ray albedo W .

For simplicity, we set many of the model parameters at reasonable values. For example, we assume the secondary star is in synchronous rotation and completely fills its Roche lobe since there is ongoing mass transfer. We initially fix the mass ratio at $Q = 2.94$, the value found by CCK98. Thus the only remaining geometrical parameter is the inclination i . Based on the secondary star's spectral type (A9III, CCK98) we fix its polar temperature at 7000K. We use limb darkening coefficients taken from Wade & Rucinski (1985). The secondary star has a radiative envelope, so the gravity-darkening exponent was set to 0.25 (von Zeipel 1924).

3.2 Upper and lower bounds on the inclination

We begin the light curve fitting by considering a simple model first. We fit the B and V light curves separately to a model with no disc light and no X-ray heating. The only free parameter is the inclination i . In this case, the best derived value of i is a lower limit since the amplitude of the light curve gets smaller as the inclination is decreased or if extra light from the accretion disc is added. We find $i \geq 42^\circ$ for B and $i \geq 49^\circ$ for V . Thus we adopt $i \geq 49^\circ$ as a lower limit. The upper limit on i based on the lack of X-ray eclipses is $i \leq 73^\circ$ (for a mass ratio of $Q = 2.94$, see CCK98). We therefore conclude $49^\circ \leq i \leq 73^\circ$.

3.3 Addition of disc light

We now consider models where light from the disc is accounted for. The disc parameters discussed above specify the disc radius, thickness, the temperature of the rim, and temperature profile. At each phase, the disc is divided up into a grid of 6300 surface elements (90 divisions in azimuth times 70 divisions in the radial direction). The local intensities are computed assuming blackbody spectra (with corrections for limb darkening) at 128 different wavelengths. The observed flux at each wavelength from the disc is obtained by summing over all of the visible surface elements, creating a model disc ‘‘spectrum.’’ The model disc spectrum is added to the model star spectrum (constructed in a similar way with local blackbody spectra and limb darkening corrections), creating the ‘‘composite’’ spectrum. This composite spectrum is integrated with the standard normalized $UBVRI$ filter response functions to obtain the final model $UBVRI$ fluxes. This method of computing the final fluxes is more precise than simply computing the fluxes at the ‘‘effective’’ wavelengths of the filters because the effective wavelengths of the filters depend on the exact shape of the input spectrum. This technique also can easily handle cases where the disc spectrum has a rather different shape than the stellar spectrum.

In cases where one has observations in several filters, the value of the radial exponent, ξ can be quite well constrained (Orosz & Bailyn 1997). However, in the case of Cyg X-2 where we only have B and V light curves, we found that the value of ξ was not well constrained (additional observations in R and I would help constrain ξ , see below). We therefore initially fixed ξ at $\xi = -0.75$, which is the value appropriate for a steady-state disc (Pringle 1981).

3.4 Addition of X-ray heating

We argue that even though Cyg X-2 is a strong X-ray source, X-ray heating is relatively unimportant with regards to the Cyg X-2 optical light curves. It is well known that strong X-ray heating of the secondary star in an X-ray binary can lead to distortions in the secondary star's observed radial velocity curve (e.g. Bahcall, Joss, & Avni 1974) and to changes in the observed spectral type of the secondary as a function of orbital phase (e.g. Crampton & Hutchings 1974). However, in the case of Cyg X-2, no distortions in the radial velocity curve or changes in the spectral type were observed by CCK98. X-ray heating of the secondary star can also alter the observed optical light curve by adding light near the photometric phase 0.5 (Avni 1978). There is no evidence for any significant excess light near $\phi = 0.5$ in the folded light curves displayed in Figure 3. There are two main reasons why X-ray heating seems to be unimportant in Cyg X-2. First of all, Cyg X-2 has a much larger orbital separation than other X-ray binaries such as Her X-1, so the X-ray flux (i.e. the number of X-ray photons per unit surface area) at the surface of the Cyg X-2 secondary star will be smaller. Secondly, many X-ray binaries are thought to have relatively thick accretion discs (e.g. Motch et al. 1987; de Jong, Augusteijn & van Paradijs 1996). The thick discs may shield the secondary star from much (if not most) of the X-rays from the central source. The accretion disc may also be warped (e.g. Wijers & Pringle 1998), in which case the secondary star may be shielded from the X-rays from the central source.

Because X-ray heating is a small effect here, we will use a simplified computational procedure. We assume that all of the X-rays come from a point centred on the neutron star. The flux of X-rays on each point on the secondary star that can see the central X-ray source is

$$F_{\text{irr}} = \Gamma \frac{L_x}{d^2}, \quad (2)$$

where d is the distance between the point in question and the centre of the neutron star, L_x is the X-ray luminosity of the central source, and where Γ is cosine of the angle between the surface normal and the direction to the central source. The rim of the accretion disc can shield the points on the secondary star that are near the orbital plane, preventing them from seeing the X-rays from the central source. $F_{\text{irr}} = 0$ in these cases. The flux of X-ray photons on a particular surface element on the secondary star (specified by the coordinates (x, y, z)) causes the local temperature to rise according to

$$T_{X\text{-ray}}^4(x, y, z) = T_{\text{pole}}^4 \left[\frac{g(x, y, z)}{g_{\text{pole}}(x, y, z)} \right]^{4\beta} + \frac{WF_{\text{irr}}}{\sigma}. \quad (3)$$

W is the X-ray albedo, g is the gravity, and σ is the Stefan-Boltzmann constant (Zhang et al. 1986; Orosz & Bailyn 1997). We see that the amount the local temperature is raised depends on the value of the product WF_{irr} . Thus it is possible to derive different values of L_x by using different values of W —the final model light curves are identical as long as the product WF_{irr} remains constant. It is also possible to obtain larger values of L_x by using a thicker accretion disc, since thicker accretion discs would shield larger parts of the secondary star. However, in this case, the final model light curves do have subtle differences. We adopt an X-ray

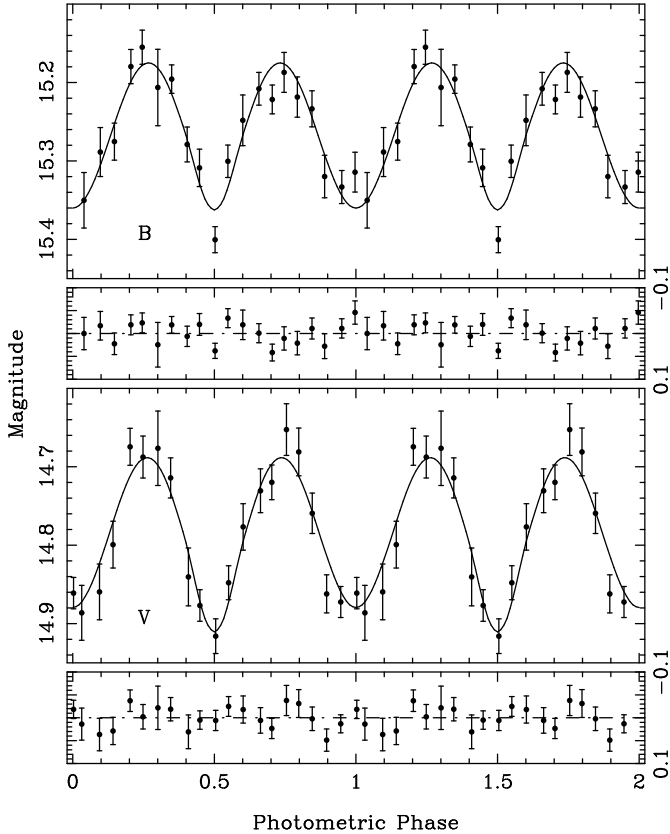


Figure 4. From top to bottom: The folded B light curve and the best-fitting model (Table 3); the B residuals in the sense of the data minus the model fit; the folded V light curve and the best-fitting model; and the V residuals. Each point has been plotted twice.

albedo of $W = 0.50$ definiteness and initially fix the X-ray luminosity at $\log L_x = 38.3$, which is roughly the Eddington luminosity for a $1.5 M_\odot$ neutron star.

3.5 Light curve fitting and computation of confidence regions

We fit the B and V light curves simultaneously. Models using a wide range of the input parameters were computed and parameters sets which gave relatively low values of χ^2 were noted. Two different optimization routines were used: one based on the “grid search” algorithm and one based on the Levenberg-Marquardt algorithm (both adopted from Bevington 1969). The optimization routines were then started using each of these parameter sets as an initial guess. Our best-fitting model (arrived at after several weeks of computation) is shown in Figure 4. Table 3 gives the values of the free parameters (which are the inclination i , the radius of the disc as a fraction of the Roche lobe radius r_d , the opening angle of the disc β_{rim} , and the temperature of the outer edge of the disc T_d). The model fits reasonably well, with $\chi^2 = 40.93$ for 36 degrees of freedom. The standard deviations of the residuals are 0.024 mag for B and 0.026 mag for V . We are reasonably certain the global χ^2 minimum

Table 3. The model parameters for the light curves shown in Figure 4 (steady-state disc case)

Parameter	Value	Comment
Q	2.94	fixed
i	$62.5^\circ \pm 4^\circ$	free
r_d	0.90 ± 0.15	free
β_{rim}	$15.04^\circ \pm 0.07^\circ$	free
T_d (K)	3950 ± 880	free
ξ	-0.75	fixed
W	0.5	fixed
$\log L_x$ (cgs)	38.3	fixed

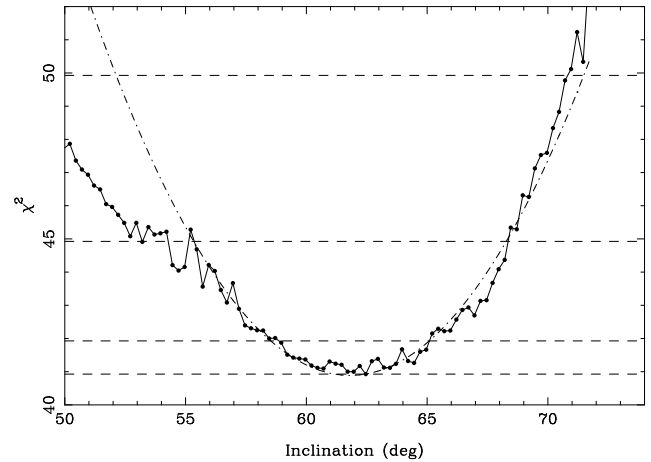


Figure 5. χ^2 vs. i for a mass ratio of $Q = 2.94$ (solid line and filled circles). The horizontal dashed lines correspond to $\chi^2 = \chi_{\text{min}}^2$, $\chi^2 = \chi_{\text{min}}^2 + 1$, and $\chi^2 = \chi_{\text{min}}^2 + 4$, and $\chi^2 = \chi_{\text{min}}^2 + 9$. The dash-dotted line is a parabola fitted to the χ^2 values between 55° and 70° .

was found, based on the large amount of parameter space searched.

The parameter errors given in Table 3 were computed with the Levenberg-Marquardt optimizer program. The sizes of the errors depend on the sizes of the parameter increments one uses to compute the numerical derivatives. As a check on these errors, we also estimated 1σ and 2σ confidence regions in the following way. A grid in the inclination-mass ratio plane was defined with inclinations between 49° and 74° in steps of 0.25° and mass ratios of 2.66, 2.94 and 3.22. Then the light curves were fit with the inclination and mass ratio fixed at the values corresponding to each grid point. In each case, the other parameters were allowed to vary until χ^2 was minimized. This iteration was started at the point where $i = 62.46^\circ$ and $Q = 2.94$. Then the fit was optimized at a neighbour point using the parameters at the lowest neighbour point as the initial guess for the optimization routine. The iteration was continued until the entire grid was filled up. We found that the value of χ^2 did not depend strongly on the mass ratio for a given inclination. We show in Figure 5 χ^2 vs. i for $Q = 2.94$ (the solid line and filled points). We also show a parabolic fit to the χ^2 values between 55° and 70° (dash-dotted line). This fit shows that the χ^2 vs. i curve is roughly parabolic near the minimum. We see that $\chi^2 = \chi_{\text{min}}^2 + 1$ at $i \approx 59^\circ$ and at $i \approx 65^\circ$. Thus $59^\circ \leq i \leq 65^\circ$

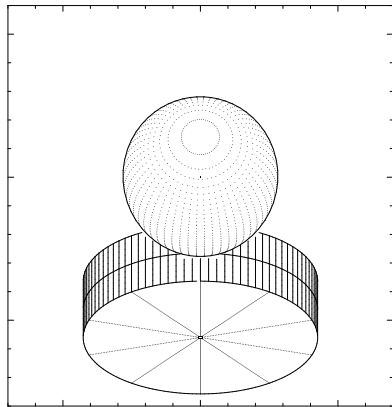


Figure 6. A schematic of the binary system as it appears on the plane of the sky at phase 0.0 for the model parameters given in Table 3.

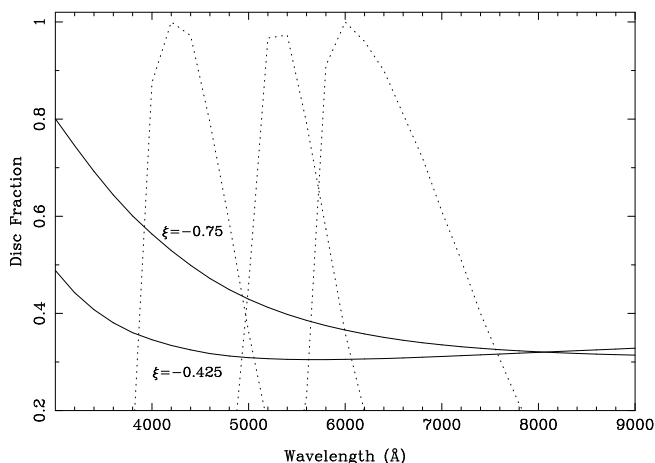


Figure 7. The disc fraction as a function of wavelength for the $\xi = -0.75$ model and for the $\xi = -0.425$ model (solid lines). The dotted lines show the filter response functions for the standard *B*, *V*, and *R* filters.

is an approximate 1σ confidence region. A rough 2σ confidence region is $56^\circ \leq i \leq 68^\circ$ where $\chi^2 = \chi_{\min}^2 + 4$ at the endpoints. The value of χ^2 increase sharply as the inclination grows beyond $\approx 68^\circ$ since the model predicts deep eclipses that are not observed. The rough 1σ errors of $\pm 3^\circ$ are not too different from the 1σ errors of $\pm 4^\circ$ computed from the Levenberg-Marquardt program. We will adopt 1σ errors of $\pm 4^\circ$ for the sake of discussion below.

3.6 The system geometry: A grazing eclipse of the disc?

We show in Figure 6 a schematic diagram of the binary system (using the model parameters given in Table 3) as it appears on the plane of the sky at phase 0.0. In this ge-

ometry we expect a grazing eclipse of the disc. The grazing eclipse of the disc results in a *V* light curve that is ≈ 0.02 mag deeper at the photometric phases 0.0 and 0.5 than the uneclipsed light curve. In principle, one would expect to observe characteristic changes in the disc emission line profile (e.g. $H\alpha$) as a function of phase for eclipsing systems (Young & Schneider 1980). However, it is not clear if the predicted grazing eclipse in Cyg X-2 is deep enough to lead to easily observable changes in the $H\alpha$ line profile. Future spectroscopic observations at the correct orbital phases may help to further constrain the inclination if one could show that partial eclipses do or do not occur.

3.7 Changes in the disc temperature profile and secondary star temperature

We did some numerical experiments to explore how the model fits depend on the parameter ξ . The reason for these experiments is that the disc in Cyg X-2 is probably strongly irradiated by the central X-ray source, and it is likely that the temperature profile of the disc is changed. Vrtilik et al. (1990) showed that the temperature profile of an irradiated accretion disc is like $T(r) \propto r^{-3/7}$ rather than the familiar $T(r) \propto r^{-3/4}$ for a steady-state non-irradiated disc. [Recently, Dubus et al. (1998) argued that a non-warped disc irradiated by a point X-ray source powered by accretion is unchanged by the irradiation. The observation that the accretion discs in most LMXBs are effected by irradiation leads Dubus et al. (1998) to conclude that the discs are either warped or that the central X-ray source is not point-like.] We computed models where the parameter ξ was fixed at several values between -0.425 and -0.750 and where the other parameters were adjusted to minimize χ^2 (the mass ratio was fixed at $Q = 2.94$). As ξ moves from -0.75 to -0.425 , the value of χ^2 of the fit increases and the best-fitting value of the inclination i decreases. When $\xi = -3/7 \approx -0.425$, $i = 54.6^\circ$ and $\chi^2 = 48.4$ for 36 degrees of freedom. We did not estimate confidence regions for the inclination for the case when $\xi = -3/7$.

We also computed models where the polar temperature of the secondary star was slightly altered from its nominal value of 7000 K. When $T_{\text{pole}} = 6700$ K (corresponding roughly to a spectral type of F2), the best-fitting inclination was $i = 63.6^\circ$ with $\chi^2 = 40.90$ for 36 degrees of freedom, slightly lower than the value of 40.93 found above for the model with $T_{\text{pole}} = 7000$ K. When $T_{\text{pole}} = 7400$ K (corresponding roughly to a spectral type of A7), the best-fitting inclination was $i = 61.5^\circ$ with $\chi^2 = 41.35$ for 36 degrees of freedom. Thus our results do not depend strongly on the adopted value of the secondary star's polar temperature.

3.8 Comparison of observed and model disc fraction

We have an independent check on the light curve models. Since the spectrum of the star and the spectrum of the disc are computed separately, we can easily predict what fraction of the flux at a given wavelength is due to the disc (we refer to this number as the “disc fraction” and denote it by k). Observationally, the disc fraction in a given bandpass can be measured using the optical spectrum of the source

and the spectra of suitable template stars (Marsh, Robinson, & Wood 1994). We obtained two spectra of Cyg X-2 1997 on November 1 and 3 with the 2.7m telescope at the McDonald Observatory (Fort Davis, Texas) using the Large Cass Spectrograph, a 600 groove/mm grating (blazed at 4200 Å), and the T11 800 × 800 CCD. The spectral resolution is ≈ 3.5 Å (FWHM) with wavelength coverage 3525–4940 Å. The signal-to-noise ratios are ≈ 50 per pixel near the He II emission line at 4686 Å. We also observed the A9III star HR 2489 on both nights. CCK98 found that the spectrum of this star best matched the absorption line spectrum of Cyg X-2. We normalized each spectrum to its continuum fit and applied the technique of Marsh, Robinson, & Wood (1994) to decompose the spectra of Cyg X-2 into the disc and stellar components. We found a disc fraction of $k_B = 0.36 \pm 0.05$ from the November 1 spectrum (orbital phase = 0.65) and $k_B = 0.37 \pm 0.05$ for the November 3 spectrum (orbital phase = 0.85). We note that these estimates of k_B represent an average value over most of the B bandpass. For comparison, J. Casares (private communication) finds from the much higher quality spectra published in CCK98 that the disc fraction in the B and R bands was variable, with $0 \lesssim k_B \lesssim 0.30$ and $0 \lesssim k_R \lesssim 0.40$ for the B and R bands, respectively. For this discussion we adopt $k_B = 0.30$ and $k_R = 0.30$.

We show in Figure 7 the model disc fraction as a function of wavelength for two models: the best-fitting solution with $\xi = -0.75$ and the best-fitting solution with $\xi = -0.425$. We also show the standard B , V , and R filter response functions. The disc fractions for the $\xi = -0.75$ model are $k_B \approx 0.55$ and $k_R \approx 0.35$. Both of these values are somewhat larger than the observed values. The disc fractions in B and R for the $\xi = -0.425$ model are slightly larger than ≈ 0.3 , much closer to the upper ranges of the observed values. However, the fit for the $\xi = -0.425$ model is worse than the fit for the $\xi = -0.75$ model ($\chi^2 = 48.44$ compared to $\chi^2 = 40.92$ for 36 degrees of freedom).

3.9 The puzzling lack of X-ray heating

We have argued above that X-ray heating of the secondary star in Cyg X-2 is not a large effect since there is no observed change in the spectral type as a function of orbital phase and because there does not appear to be a large amount of excess light at the photometric phase 0.5. The effect of the X-ray heating in the model given in Table 3 is small—there is about ≈ 0.01 to 0.02 magnitudes of excess light added near phase 0.5 compared to the light curve without heating. This is in spite of the fact that the neutron star is accreting at nearly the Eddington rate (see Smale 1998). In our model the rim of the disc shields most of the secondary star from the central X-ray source [although it is also likely that the disc is warped (Dubus et al. 1998), our model currently only uses an axisymmetric disc].

It turns out that solving the “problem” of no X-ray heating of the secondary star leads to another puzzle. Namely, it is clear observationally that the disc in Cyg X-2 is slightly fainter in the optical than the secondary star (i.e. the observed disc fractions in B and R are ≈ 0.3). However, Jan van Paradijs pointed out to us that relative faintness of the disc is somewhat surprising since one would expect a substantial amount of light from the reprocessing of the

X-rays absorbed by the disc. The He II $\lambda 4868$ Å line is in emission, so presumably there is at least some X-ray reprocessing. Based on the relations given in van Paradijs & McClintock (1994), the absolute V magnitude of the accretion disc should be $M_V = -2.02 \pm 0.56$. We compute $M_V = 0.38 \pm 0.35$ for the disc, based on our model parameters (the secondary star by itself has $M_V = -0.54 \pm 0.24$, see Section 4.2). Thus the disc in Cyg X-2 is about a factor of 9 fainter in V than expected based on the simple scaling laws given in van Paradijs & McClintock (1994). It is possible that much of the reprocessed flux from the disc is emitted at shorter wavelengths than B , which might account for some of the mismatch between the observed and expected disc brightness.

Presently, the code does not self-consistently account for optical flux from the disc due to reprocessing of absorbed X-rays. The brightness of the disc is set based on the temperature at the outer edge, the radial temperature profile, and the disc radius, and is independent on the adopted value of L_x . The code is “flexible” in the sense that the power-law exponent on the temperature radial profile can be adjusted to approximate the changes in the disc caused by irradiation. As we showed above, the model disc fractions are not too different than what is observed. It therefore appears that this lack of a self-consistent computation of the disc flux is not a major problem.

3.10 Summary of model fitting and discussion

The fits to the B and V light curves are better if we assume that the disc is in a steady state where $T(r) \propto r^{-0.75}$. However, in this case the model disc is bluer than what is observed since our predicted disc fraction in B ($k_B \approx 0.55$) is larger than what is observed ($k_B \approx 0.30$). If we assume that the disc is strongly irradiated so that $T(r) \propto r^{-0.425}$, then the model disc is redder and the predicted disc fraction in B ($k_B \approx 0.32$) is closer to what is observed. However, in this case, the χ^2 of the fit is much worse ($\chi^2 = 48.4$ compared to $\chi^2 = 40.9$ with 36 degrees of freedom for the steady-state case). Fortunately, the best-fitting values of the inclination are not that different in the two cases: $i \approx 62.5^\circ$ for the steady-state disc case and $i \approx 54.6^\circ$ for the irradiated case, which is in the 2σ range of the steady-state disc case. For the sake of the discussion in Section 4 we adopt the 1σ inclination from the steady-state case ($i = 62.5^\circ \pm 4^\circ$, where we assume the errors are Gaussian) because of the lower χ^2 .

It is important to recall here that observed optical light curves consist mainly of two components: the light from the distorted secondary star and the light from the accretion disc. We have argued that there is very little extra light due to X-ray heating of the secondary star. We assume that the light from the secondary star is modulated in phase while the light from the disc is not (with the possible exception of a grazing eclipse). Thus to model the observed light curves we should compute the relative amounts of disc light and secondary star light at each observed wavelength region for every observed phase.

In our current model we compute the disc light at every observed wavelength region by specifying four parameters: the disc radius in terms of the neutron star Roche lobe radius, the opening angle of the disc rim, the temperature profile of the disc, and the temperature of the disc rim. The flux

at each grid point across the disc is computed from the local temperature assuming a blackbody spectrum. The code does not account for flux from the disc due to reprocessing of absorbed X-rays from the central source. Typically, the spectrum of the disc (in the optical) will have a rather different shape than the spectrum of the secondary star. Hence one should have observed light curves in as many wavelength bands as possible in order to better determine the shapes of the disc and stellar spectra. Eclipsing systems with well-defined and smooth light curves like GRO J1655-40 (Orosz & Bailyn 1997; van der Hooft et al. 1998) offer additional constraints on the disc radius, thickness, and temperature.

On the other hand, there is no particular reason to adopt our parameterization of the disc since the important quantity is the relative amount of disc and star light at a particular wavelength. In fact, by using suitably high quality spectra one could simply measure the disc fraction k_λ at several different wavelengths covering the bandpasses of the observed light curves. In this case the model disc spectrum would be constructed from the model star spectrum since the quantity $k_\lambda = f_{\text{disc}}/(f_{\text{disc}} + f_{\text{star}})$ is known at each wavelength point (here f_{disc} and f_{star} refer to the model fluxes from the disc and star, respectively, at a given orbital phase). Then, as before, the model disc spectrum is added to the model star spectrum and the resulting composite spectrum is integrated with the filter response curves to produce model fluxes in each bandpass. Thus one could eliminate the model parameters T_d and ξ . We note that one still needs a model disc to account for the effects of X-ray shadowing by the disc rim and possibly the slight loss of flux due to the eclipse, so the model parameters β_{rim} and r_d are still needed.

Thus, future modelling of the Cyg X-2 light curves can be improved by observing the light curves in more colours (i.e. at least in B , V , R , and I and possibly also in the infrared), and by obtaining quasi-simultaneous spectroscopic observations of Cyg X-2 and template stars over a wide wavelength range. In practice, one needs observations over many orbital cycles in order to average out the variations in the observed disc fraction and to define the lower light curve envelopes.

4 DISCUSSION

4.1 Mass of the neutron star

The masses of the neutron star and secondary star can be computed from the optical mass function, the mass ratio, and the inclination (CCK98):

$$M_x = \frac{f(M)(1+q)^2}{\sin^3 i} = (1.24 \pm 0.09 M_\odot)(\sin i)^{-3}. \quad (4)$$

Using our 1σ limits on the inclination ($i = 62.5^\circ \pm 4^\circ$) we find $M_x = 1.78 \pm 0.23 M_\odot$ and $M_c = 0.60 \pm 0.13 M_\odot$. The extreme range of allowed inclinations ($49^\circ \leq i \leq 73^\circ$) implies an extreme mass range allowed for the neutron star of $1.42 \pm 0.10 M_\odot \leq M_x \leq 2.88 \pm 0.21 M_\odot$.

Since the values of the optical mass function and the mass ratio were fairly well determined by CCK98, the largest uncertainty on M_x is the value of the inclination i one chooses. Thus it is instructive to see how the mass of the neutron star varies as a function of the inclination. We plot in Figure 8 the mass of the neutron star as a function of the

inclination. We also indicate the 1σ errors at several different inclinations. The mass of the neutron star in Cyg X-2 is consistent at the 1σ level with the canonical neutron star mass of $1.35 M_\odot$ (Thorsett & Chakrabarty 1998) for inclinations greater than 70° . However, the fits to the light curves get increasingly worse as the inclination grows larger than $\approx 68^\circ$ (i.e. the sharp increase in χ^2 displayed in Figure 5), so it is unlikely that the inclination of Cyg X-2 is much larger than $\approx 68^\circ$. At the lower value of the 1σ inclination range for our model with the unirradiated disc ($i = 58.5^\circ$), the neutron star mass is $M_x = 2.00 \pm 0.15 M_\odot$, which is more than 4σ larger than the canonical mass of $1.35 M_\odot$.

For most of the parameter space in i , $f(M)$, and q , the mass of the neutron star in Cyg X-2 exceeds the average mass of the neutron stars in binary radio pulsars. Thus Cyg X-2 contains a rare example of a “massive” neutron star. Perhaps the best-known example of a massive neutron star is the high-mass X-ray binary Vela X-1 (4U 0900-40). Vela X-1 is an eclipsing system, and the neutron star is an X-ray pulsar. Dynamical mass measurements by van Kerkwijk et al. (1995b) gave a mass of $M_x = 1.9_{-0.5}^{+0.7}$ (95% confidence limits). A later analysis of IUE spectra by Stickland et al. (1997) gave a mass consistent with $1.4 M_\odot$ ($1.34 M_\odot \lesssim M_x \lesssim 1.53 M_\odot$). However, a recent reanalysis of the UV data (Barziv et al. 1998, in preparation) gives $M_x = 1.9 M_\odot$, consistent with the result of van Kerkwijk et al. (1995b). Barziv et al. (1998, in preparation) also find $M_x = 1.9 M_\odot$ from optical spectra. The range of derived masses by different groups is an indication of the difficulty in analyzing the radial velocity curves of a high-mass companion star such as the one in Vela X-1. Another example of a possible massive neutron star is the eclipsing high-mass X-ray binary 4U 1700-37. The companion star (HD 153919) is an O6f star with a strong wind. Heap & Corcoran (1992) find $M_x = 1.8 \pm 0.4 M_\odot$. However, 4U 1700-37 does not pulse and its X-ray spectrum is harder than the spectra of typical X-ray pulsars. This lack of “neutron star signatures” has led Brown, Weingartner, & Wijers (1996) to speculate that 4U 1700-37 contains a “low-mass” black hole rather than a neutron star.

Recent computations of the neutron star and black hole initial mass function by Timmes, Woosley, & Weaver (1996) indicate that Type II supernovae give rise to a bimodal distribution of initial neutron star masses. The average masses for the two peaks are $1.26 \pm 0.06 M_\odot$ and $1.73 \pm 0.08 M_\odot$, respectively. Type Ib supernovae tend to produce neutron stars in the lower mass range. The masses derived by Timmes et al. (1996) do not include mass that may fall back onto the neutron star shortly after the supernova explosion. The mean mass for the lower-mass distribution of $1.26 \pm 0.06 M_\odot$ agrees well with the mean mass of the binary radio pulsars of $1.35 \pm 0.04 M_\odot$ determined by Thorsett & Chakrabarty (1998). The mass of the neutron star in Cyg X-2 seems to be significantly larger than both of these masses. However, the neutron star mass of $M_x = 1.78 \pm 0.23 M_\odot$ given above agrees well with the mean mass of $1.73 \pm 0.08 M_\odot$ derived by Timmes et al. (1996) for the higher-mass peak of their bimodal distribution. Thus the current mass of the neutron star in Cyg X-2 might simply be the mass at its formation (within the framework of the models of Timmes et al. (1996)). Alternatively, Zhang, Strohmayer, & Swank (1997) point out that one would expect massive neutron stars to

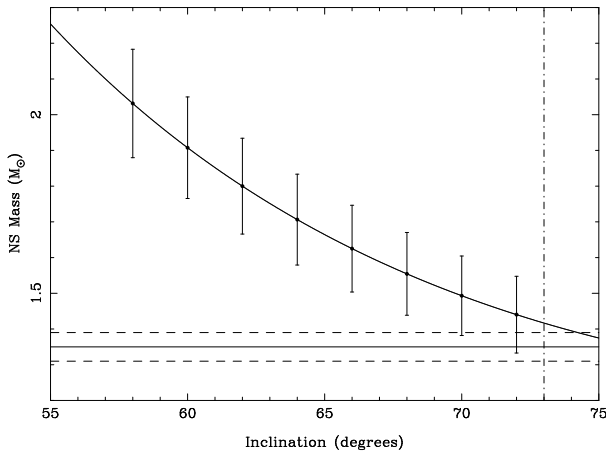


Figure 8. The mass of the neutron star as a function of the inclination is shown. We assume an optical mass function of 0.69 ± 0.03 and a mass ratio of $M_c/M_x = 0.34 \pm 0.04$ (CCK98). The vertical line indicates the upper limit on the inclination imposed by the lack of observed X-ray eclipses. The horizontal lines indicate the canonical neutron star mass of $1.35 \pm 0.04 M_\odot$ found from the binary radio pulsars.

exist in systems where a neutron star formed at $\approx 1.4 M_\odot$ has been accreting at the Eddington rate for extended periods of time. If the kilohertz QPOs observed in Cyg X-2 and other neutron star LMXBs can be interpreted as the frequency of the last stable orbit of the inner accretion disc, then the neutron star masses in some X-ray binaries could be as large as $\approx 2 M_\odot$. Assuming the neutron stars were formed at $\approx 1.4 M_\odot$, the $\approx 0.6 M_\odot$ of extra matter is not an unreasonable amount to accrete in $\approx 10^8$ years (Zhang et al. 1997). One would basically have to know how long Cyg X-2 has been accreting at near Eddington rates in order to determine whether the neutron star formed at “low mass” ($\approx 1.3 M_\odot$) or “high mass” ($\approx 1.7 M_\odot$). It remains to be seen if a reliable age estimate can be derived from a binary evolution model of this system.

According to King et al. (1997), a companion star mass of at least $\approx 0.75 M_\odot$ is needed to maintain steady accretion in a neutron star low-mass X-ray binary like Cyg X-2. If $M_c > 0.75 M_\odot$, then $M_x > 1.88 M_\odot$ at the 95% confidence level (CCK98), which would require an inclination lower than about 60° , near the lower end of the 1σ inclination range. We find $M_c = 0.60 \pm 0.13 M_\odot$ (1σ) using $i = 62.5^\circ \pm 4^\circ$, which is $\approx 1\sigma$ smaller than minimum M_c of King et al. (1997). The extreme range of allowed inclinations ($49^\circ \leq i \leq 73^\circ$) implies an extreme mass range allowed for the secondary star of $0.48 \pm 0.09 M_\odot \leq M_c \leq 0.98 \pm 0.18 M_\odot$. In principle, a measurement of the surface gravity of the secondary star would provide an independent estimate of M_c since the density of the Roche-lobe filling secondary star in a semi-detached binary depends only on the orbital period to a good approximation (Pringle 1985). However, one would need to measure $\log g$ to better than ≈ 0.03 dex to distinguish between $M_c = 0.60 M_\odot$ and $M_c = 0.75 M_\odot$.

4.2 The Distance to the Source

We can compute the distance to the source using the results of our model fitting. Once the inclination i is given, we can

compute the total mass of the system. The size of the semi-major axis a is then computed from Kepler’s third law. We then use Eggleton’s (1983) formula to compute the effective radius of the secondary’s Roche lobe in terms of the orbital separation a :

$$\frac{R_{Rl}}{a} = \frac{0.49q^{2/3}}{0.6q^{2/3} + \ln(1 + q^{1/3})}. \quad (5)$$

The intrinsic luminosity of the secondary star then follows from the Stefan-Boltzmann relation, where we assume $T_{\text{eff}} = 7000 \pm 250$ K and a bolometric correction of 0. To get the intrinsic luminosity of the entire system we must add light from the accretion disc. We do not have spectroscopic observations in the V band available so we will interpolate between the measurements of k_B and k_R and adopt $k_V = 0.30 \pm 0.05$. Finally, the distance modulus can be computed after we account for interstellar extinction. The most complete study of the interstellar extinction in the direction of Cyg X-2 is that of McClintock et al. (1984). They derived a colour excess of $E(B - V) = 0.40 \pm 0.07$ based on spectra from the *International Ultraviolet Explorer* and on optical photometry and spectra of 38 nearby field stars. Assuming $A_V = 3.1E(B - V)$, the 1σ A_V range of McClintock et al. (1984) is $1.02 \leq A_V \leq 1.46$. Using this A_V range, we find a distance of $d = 7.2 \pm 1.1$ kpc, where we have adopted $i = 62.5^\circ \pm 4^\circ$ and a mean apparent V magnitude of 14.8 for the “quiescent” state (Figures 3, 4). The absolute V magnitude of the system is $M_V = -0.93 \pm 0.25$, and the absolute V magnitudes of the components separately are $M_V = 0.38 \pm 0.35$ for the disc, and $M_V = -0.54 \pm 0.24$ for the secondary star, respectively. Finally, if we use the inclination derived using the irradiated disc ($i = 54.6^\circ$), then we find a distance of $d = 7.9$ kpc.

Previous distance estimates include the distance derived by Cowley et al. (1979) of $d = 8.7 \pm 2.0$ kpc, where we have propagated their estimated error on the bolometric magnitude of ~ 0.5 mag (see Smale 1998). Our distance estimate is consistent with that of Cowley et al. (1979). Recently, Smale (1998) derived a distance of 11.6 ± 0.3 kpc from observations of a type I radius-expansion burst in Cyg X-2, where he assumed a neutron star mass of $1.9 M_\odot$ to derive the Eddington luminosity of the neutron star. Our derived distance is $\approx 4\sigma$ smaller than that of Smale (1998).

To facilitate a comparison between the various distance estimates, we plot in Figure 9 the distance to Cyg X-2 as a function of the visual extinction A_V . Since the distance to the source depends weakly on the assumed inclination and somewhat strongly on the assumed disc fraction, we show four d vs. A_V curves: (1) $i = 70^\circ$, $k_V = 0.3$; (2) $i = 63^\circ$, $k_V = 0.3$; (3) $i = 63^\circ$, $k_V = 0.5$; and (4) $i = 63^\circ$, $k_V = 0.7$. The computed distance to the source decreases sharply as A_V grows larger. If the 1σ A_V range of McClintock et al. (1984) is correct ($1.02 \leq A_V \leq 1.46$), then the disc fraction must be greater than $k_V \gtrsim 0.7$ in order for the derived distance to be consistent with Smale’s (1998) measurement. However, a disc fraction of $k_V = 0.7$ is much larger than what is observed: our spectra and the spectra of CCK98 give disc fractions of $\lesssim 0.3$ in the B and R bands. If the disc fraction of $k_V = 0.3$ is correct, then the visual extinction must be rather small ($A_V \lesssim 0.2$ mag) in order to get a distance of ≈ 11 kpc. However, we note that the distance derived by Smale (1998) depends on the assumed neutron star mass

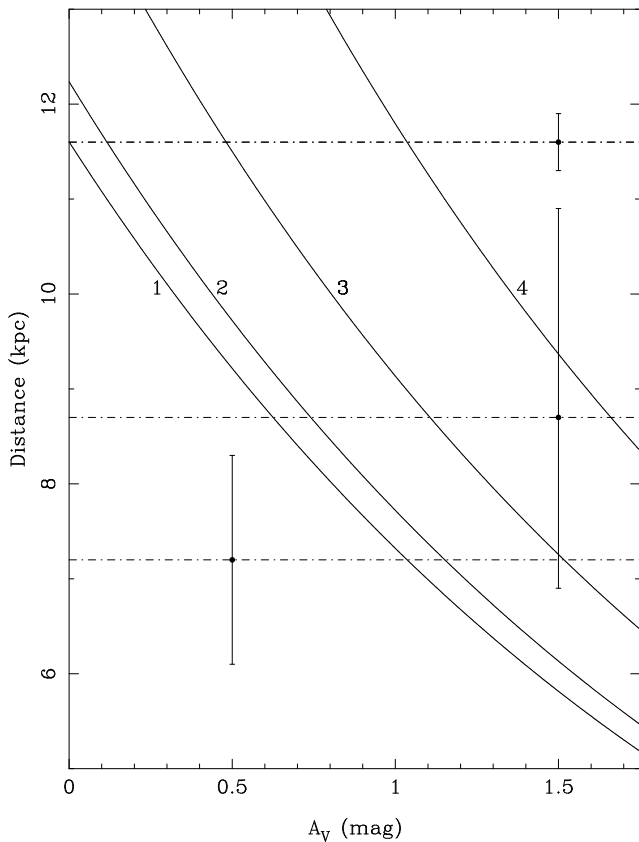


Figure 9. The distance to Cyg X-2 as a function of the visual extinction A_V . The numbered curves show the distance for four combinations of the inclination and disc fraction: (1) $i = 70^\circ$, $k_V = 0.3$; (2) $i = 63^\circ$, $k_V = 0.3$; (3) $i = 63^\circ$, $k_V = 0.5$; and (4) $i = 63^\circ$, $k_V = 0.7$. The three points with the error bars indicate the distance derived by us ($d = 7.2 \pm 1.1$ kpc), by Cowley et al. (1979, $d = 8.7^{+2.2}_{-1.8}$ kpc), and by Smale (1998, $d = 11.6 \pm 0.3$ kpc). The locations of the points along the A_V -axis have no particular meaning.

(and other parameters, e.g. Lewin, van Paradijs, & Taam 1993). If one assumes a neutron star mass of $M_x = 1.78 M_\odot$, the distance would be $d = 11.2 \pm 0.3$ kpc (using standard burst parameters). This distance is marginally consistent with the estimate of Cowley et al. (1979), but still inconsistent with our distance estimate. One needs a rather small neutron star mass ($M_x \lesssim 0.9 M_\odot$) in order to get a distance from the type I radius-expansion burst consistent with our measurement. Thus it is quite difficult to reconcile the differences between our distance estimate and that of Smale (1998).

5 SUMMARY

We have collected from the literature U , B , and V light curves of Cyg X-2. The B and V light curves show significant periodicities in their power spectra. The most significant periodicities in the B and V light curves correspond to half of the orbital period of $P = 9.8444$ days. The “quiescent”

light curves derived from the lower envelopes of the folded B and V light curves are ellipsoidal. We fit ellipsoidal models to the “quiescent” light curves; from the best-fitting model we derive a 1σ inclination range of $i = 62.5 \pm 4^\circ$, and a lower limit on the inclination of $i \geq 49^\circ$. The mass of the neutron star is $M_x = 1.78 \pm 0.23 M_\odot$, where we have used previous determinations of the mass ratio ($q = M_c/M_x = 0.34 \pm 0.04$) and the optical mass function ($f(M) = 0.69 \pm 0.03 M_\odot$), and the 1σ inclination range of $i = 62.5^\circ \pm 4^\circ$. We find a distance of $d = 7.2 \pm 1.1$ kpc, which is significantly smaller than a recent distance determination of $d = 11.2 \pm 0.3$ kpc derived from an observation of a type I radius-expansion X-ray burst (assuming $M_x = 1.78 M_\odot$), but consistent with earlier estimates.

ACKNOWLEDGMENTS

This research has made use of the Simbad database, operated at CDS, Strasbourg, France. We thank Tariq Shahbaz, Jan van Paradijs, Phil Charles, and Lex Kaper for various useful discussions and Jorge Casares for making his measurements of the disc fraction available to us.

REFERENCES

- Avni Y., 1978, in *Physics and Astrophysics of Neutron Stars and Black Holes*, eds. R. Giacconi & R. Ruffini (Amsterdam: North-Holland), 42
- Avni Y., & Bahcall J. N., 1975, *ApJ*, 197, 675
- Bahcall J. N., Joss P. C., & Avni Y., 1974, *ApJ*, 191, 211
- Basko M. M., Goranskii V. P., Lyutyi V. M., Ruzan L. L., Sunyaev R. A., Shugarov S. Yu., 1976, *Perem. Zvezdy*, 20, 219
- Beskin G. M., Neizvestnyi S. I., Pimonov A. A., Plakhotnichenko V. L., Shvartsman V. F., 1979, *SvAL*, 5, 271 (*PAZh*, 5, 508)
- Bevington P. R., 1969, *Data Reduction and Error Analysis for the Physical Sciences*. McGraw Hill, New York
- Brown G. E., Weingartner J. C., Wijers R. A. M. J., 1996 *ApJ*, 463, 297
- Casares J., Charles P., Kuulkers E., 1998, *ApJ*, 493, L39 (CCK98)
- Chevalier C., Bonazzola S., Ilovaisky S. A., 1976, *A&A*, 53, 313
- Cowley A. P., Crampton D., Hutchings J. B., 1979, *ApJ*, 231, 539
- Crampton D. & Hutchings J. B. 1974, *ApJ*, 191, 483
- Crampton D., Cowley A. P., 1980, *PASP*, 92, 147
- Dubus G., Lasota J.-P., Hameury J.-M., Charles P. A., 1998, *MNRAS*, in press (astro-ph/9809036)
- Eggleton P. P., *ApJ*, 268, 368
- Giacconi R., Gorenstein P., Gursky H., Usher P., Waters J. R., Sandage A. R., Osmer P., & Peach J., 1967, *ApJ*, 148, L129
- Goranskii V. P., Lyutyi V. M., 1988, *SvA*, 32, 193
- Heap S. R., Corcoran M. F., 1992, *ApJ*, 387, 340
- Homer L., Charles P. A., Naylor T., van Paradijs J., Ariere M., Koch-Miramond L., 1996, *MNRAS*, 282, L37
- Ilovaisky S. A., Chevalier C., Chevreton M., Bonazzola S., 1978, *A&A*, 67, 287
- Kahn S. M., Grindlay, J. E., 1984, *ApJ*, 281, 826
- Kilyachkov N. N., 1978, *SvAL*, 4, 217
- King A. R., Frank J., Kolb U., Ritter H., 1997, *ApJ*, 484, 844
- Kong A. K. H., Charles P. A., Kuulkers E., 1998, *NewA*, 3, 301
- Kristian J., Sandage A., Westphal J. A., 1967, *ApJ*, 150, L99
- Kuulkers E., van der Klis M., van Paradijs J., 1995, *ApJ*, 450, 784
- Lewin W. H. G., van Paradijs J., Taam R. E., 1993, *SSR*, 62, 223
- Lyutyi V. M., Sunyaev R. A., 1976, *SvA*, 20, 290

- Marsh T. R., Robinson E. L., & Wood J. H., 1994, MNRAS, 266, 137
- McClintock J. E., Petro L. D., Hammerschlag-Hensberge G., Proffitt C. R., & Remillard R. A., 1984, ApJ, 283, 794
- Motch C. et al., 1987, ApJ, 313, 792
- Mumford G. S., 1970, IAU Symp. 37, p. 177
- Orosz J. A., & Bailyn C. D., 1997, ApJ, 477, 876 (Erratum: ApJ, 482, 1086)
- Pavlenko E. P., Martin A. C., Casares J., Charles P. A., Ketsaris N. A., 1996, MNRAS, 281, 1094
- Peimbert M., Spinrad H., Taylord B. J., Johnson H. M., 1968, ApJ, 151, L93
- Pringle J. E., 1981, ARA&A, 19, 137
- Pringle J. E., 1985, in Pringle J. E., Wade, R. A., Interacting Binary Stars, Cambridge University Press, Cambridge, p. 1
- Smale A. P., 1998, ApJ, 498, L141
- Stairs I. H., Arzoumanian Z., Camilo F., Lyne A. G., Nice D. J., Taylor J. H., Thorsett S. E., & Wolszczan A., 1998, ApJ., in press
- Stickland D., Lloyd C., & Radziun-Woodham A., 1997, MNRAS, 286, L21
- Thorsett S. E., Chakrabarty D., 1998, ApJ, in press (astro-ph/9803260)
- Timmes F. X., Woosley S. E., Weaver T. A., 1996, ApJ, 457, 834
- van der Hooft F., et al., 1998, A&A, 329, 538
- van Kerkwijk M. H., van Paradijs J., & Zuiderwijk E. J., 1995a, A&A, 303, 497
- van Kerkwijk M. H., van Paradijs J., Zuiderwijk E. J., Hammerschlag-Hensberge G., Kaper L., & Sterken C. 1995b, A&A, 303, 483
- van Paradijs J., McClintock J. E., 1994, A&A, 290, 133
- van Paradijs J., 1998, in Buccheri R., van Paradijs J., Alper M. A., The Many Faces of Neutron Stars, Kluwer Academic Publishers, in press (astro-ph/9802177)
- Vrtilek S., et al., 1990, A&A, 235, 162
- von Zeipel H., 1924, MNRAS, 84, 665
- Wade R. A., & Rucinski S. M., 1985, A&AS, 60, 471
- Wijers R. A. M. J., Pringle J. E., 1998, submitted to MNRAS (astro-ph/9811056)
- Wijnands R. A. D., Kuulkers E., Smale A. P., 1996, ApJ, 473, L45
- Young P. J., Schneider D. P., 1980, ApJ, 238, 955
- Zhang E.-H., Robinson E. L., Stover R. E., 1986, ApJ, 305, 740
- Zhang W., Strohmayer T. E., Swank J. H., 1997, ApJ, 482, L167

This paper has been produced using the Royal Astronomical Society/Blackwell Science L^AT_EX style file.